V European Conference on Computational Fluid Dynamics
ECCOMAS CFD 2010
J. C. F. Pereira and A. Sequeira (Eds)
Lisbon, Portugal,14-17 June 2010

ANALYSIS OF THE TEMPORAL FLOW FIELD IN A TRACHEOBRONCHIAL MODEL

W. Schröder*, G. Eitel*, Th. Soodt*, A. Henze*

*Institute of Aerodynamics, RWTH Aachen University,
Wüllnerstrasse 5a, 52062 Aachen, Germany
e-mail: office@aia.rwth-aachen.de

Key words: Realistic lung geometry, pulsatile flow, respiration frequency, Lattice-Boltzmann method, secondary vortex structures

Abstract. *The pulsatile flow field in the human lung is numerically and experimentally investigated. The realistic lung geometry of a human subject was obtained down to the sixth generation of bifurcation and used as a tracheobronchial model. The numerical analysis is based on a Lattice-Boltzmann method which is particularly suited for flows in extremely intricate geometries such as the upper human airways. The measurements are performed via the particle-imaging velocimetry method in a transparent cast generated from the original dataset. Experimental and numerical results are compared and a thorough discussion of the three-dimensional flow structures emphasizes the unsteady character of the flow field. At inspiration, the primary flow shows clear separations and is highly influenced by secondary flow structures. In contrast, at expiration the primary flow distribution is far more homogeneous with a concurrent higher value of vorticity. It is evidenced that the asymmetric geometry of the human lung plays a significant role for the development of the flow field in the respiratory system. Secondary vortex structures and their temporal formation are analyzed and described in detail for two respiration frequencies, revealing that the qualitative flow phenomena are invariable if a certain mass flux rate is exceeded.*

1 INTRODUCTION

From a fluid mechanics point of view the human lung is a highly complex pipe network at progressively decreasing diameters. Besides air transport and exchange of carbon dioxide and oxygen in the pulmonary alveoli, the air has to be heated up and moisturized and solid particles are removed from the flow at inspiration. At expiration the loss of heat and humidity has to be limited. Thus, the requirements are challenging and several processes take place at the same time inside the respiratory tract.

The detailed analysis of the flow processes in the upper human airways is a must to develop aerosol drug delivery systems and to improve the efficiency and usability of artificial respiration systems. Numerous experimental and numerical investigations of lung flow have been conducted so far.[1–4] However, due to the high geometric intricacy of the human lung, there is still a considerable amount of uncertainty concerning the very complex flow field and fundamental results for realistic lung models are still rare. Many investigations are based on simplified models of the lung structure. The most popular of these models is the so-called Weibel model[5] which describes the bronchi as a symmetric tree structure of subsequent bifurcating pipes consisting of 23 generations. However, in most of the studies only the first three to five generations are considered and a planar representation is favored for simplicity. In[1] detailed experimental studies were performed for a planar Weibel model where fundamental flow phenomena like m-shaped velocity profiles and counter-rotating vortices were described. It was shown in numerical studies,[2,6] however, that the flow field for the non-planar configuration differs significantly from the planar case. Studies considering asymmetric bifurcations,[3] non-smooth surfaces[7] and CT-based models[4,8,9] show that the inspiration flow in the upper human airways is asymmetric and swirling. These results emphasize the importance of realistic airway models.

Generally, the aforementioned results show that an accurate lung geometry, i. e., CT data or a real human lung cast, is required to obtain physiologically relevant results. Grosse et al.[10,11] experimentally investigated the steady and oscillating flow field in a silicon model of a human lung cast that covers the trachea and the bronchial tree down to the sixth generation. It was found that the flow structures mainly depend on the instantaneous Reynolds number and on the Womersley number. Since in the experiment only a parallel cutting plane could be taken into account, the investigation of vortical structures was limited to a detailed qualitative analysis.

The present work focuses on the numerical investigation of the unsteady three-dimensional flow for the lung model used by Grosse et al.[10] for a normal respiration at rest and for an increased rate of respiration. Numerical results are compared with experimental findings and flow structures are described in detail. The flow field is simulated via a Lattice-Boltzmann method (LBM).[12] Unlike former numerical investigations, in which a simplified geometry was used, the present method can be efficiently applied to variable, realistic airway geometries. For instance the flow field downstream of the laryngeal region

was recently investigated in[13,14] by an LBM. In combination with an automated grid generation[15] based on CT-data this method offers an efficient tool for biomedical flow problems. Since the numerical method is capable of reproducing small-scale features of the entire lung flow, the results support to fundamentally understand respiratory mechanisms. Thus, the numerical results allow an extended analysis of the three-dimensional flow structures observed in the experiment.

The structure of this paper is as follows. First, the lung model is specified. Then, numerical and experimental results are compared and discussed. Finally, the findings are summarized and some conclusions are drawn.

2 THE LUNG MODEL

The geometry for the numerical investigations is based on a radiological scan taken from a cast of a human lung including the larger part of the trachea down to the sixth generation of the bronchial tree. The digital geometry reconstruction encompasses the pre-processing, the segmentation, the surface generation, and the iterative surface smoothing. Based upon the surface data a computational mesh is automatically generated by an in-house grid generator.

The same lung data was used to generate the silicon model for the PIV measurements in several manufacturing processes including corn starch rapid prototyping, surface coating, inlet insert attachment, transparent silicon (RTV815) casting, hot water wash-out, and manual channel drilling of the model's exits. These steps lead to models which allow flow field measurements within organic geometries and give the opportunity to understand in-vivo flow phenomena.

The geometry is simplified in the sense that any elasticity of the configuration is not considered. However, the upper airways, as they are modeled here, are supported by chondral springs and can be assumed as the stiffest part of the lung. The physiological lung is an enclosed system with spatially varying tissue properties that lead to non-linear pressure-volume relations. The resulting spatial pressure distribution yields equilibrium processes which cannot be accounted in a model having open ends. At the tracheal cross section a fully developed laminar inflow is imposed by a Dirichlet boundary condition in the numerical analysis and by an extended trachea in the experiment.

Assuming a static geometry and neglecting any compliance influence of the lower lung parts, the present method delivers a fundamental insight into the lung flow, including the propagation of ventilation, frequency dependent spatial and temporal mass flow rates, shear stresses, dead water regions, and secondary flow structures. Fig. 1(a) shows the final experimental model from a dorsal point of view and in Fig. 1(b) the model of the numerical simulation is illustrated.

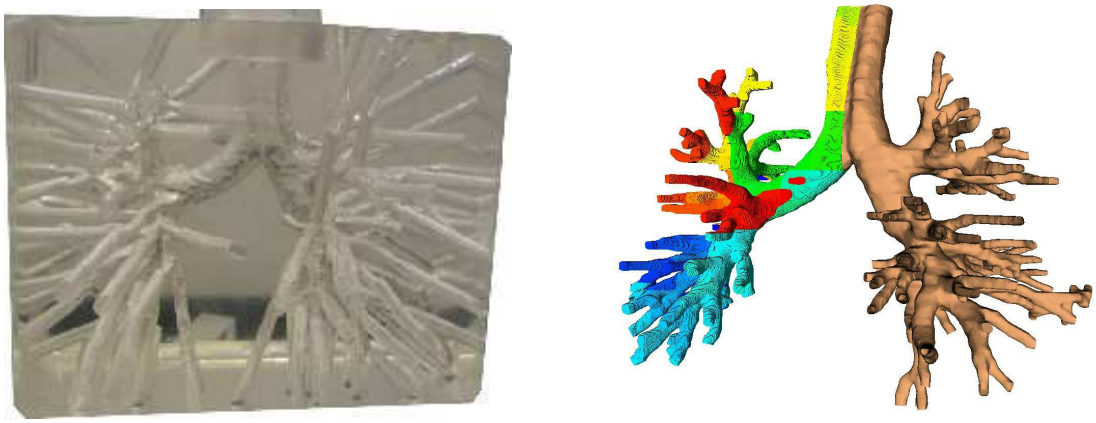

(a) (b)

Figure 1: The employed lung model: (a) silicon model for PIV measurements, (b) surface data and computational grid.

3 THE LATTICE-BOLTZMANN METHOD

Next, the Lattice-Boltzmann Method (LBM), is concisely described. The LBM is a solution algorithm for nonlinear partial differential equations and it arose from Lattice Gas Cellular Automata (LGCA) which were introduced by Frisch et al.[16] in 1986. It was shown by the authors that a microscopic model describing molecular dynamics with collisions which conserve mass and momentum leads in the macroscopic limit to the Navier-Stokes equations if the underlying lattice possesses a sufficient symmetry. An extensive description of both methods, the LGCA and the LBM, is given in.[12,17,18] The most common variant of the LBM is based on the Boltzmann equation with a simplified collision operator proposed by Bhatnagar, Gross, and Krook[19] called BGK equation. The velocity space is discretized into a set of n molecular velocities $\boldsymbol{c}_i$ with their associated distribution functions $f_i(\boldsymbol{x}, t)$. The discrete BGK equation without external forcing reads

$$f_i(\boldsymbol{x} + \boldsymbol{c}_i \Delta t, t + \Delta t) - f_i(\boldsymbol{x}, \boldsymbol{t}) = \omega \left(f_i^{eq} - f_i \right) , \tag{1}$$

where f^{eq} is the Maxwell equilibrium distribution function and ω represents the collision frequency. The corresponding numerical method is referred to as LBM-BGK method. The left-hand side of Eq. 1 contains the temporal change and the propagation term, whereas the right-hand side describes molecular collisions by a relaxation of the distribution functions towards thermodynamic equilibrium. Therefore, the algorithm of the flow solver is based on the iterative computation of propagation and collision processes for all cells of the computational grid. The macroscopic values of density ρ and momentum $\boldsymbol{j}$ are obtained as base moments of the distribution function which read

$$\rho(\boldsymbol{x},t) = \sum_{i=1}^{n} F_i(\boldsymbol{x},t) \tag{2}$$

$$\boldsymbol{j}(\boldsymbol{x},t) = \rho(\boldsymbol{x},t)\boldsymbol{v}(\boldsymbol{x},t) = \sum_{i=1}^{n} \boldsymbol{c}_i F_i(\boldsymbol{x},t)\,. \tag{3}$$

The LBM-BGK describes weakly compressible flows at moderate Reynolds numbers and it has been shown in the literature[20] that it yields indeed solutions to the Navier-Stokes equations. LBM models are characterized by the number of spatial dimensions m and the number of discrete velocities n. Therefore, the DmQn notation was introduced by Qian et al.[21] Favored models in two and three dimensions are D2Q9, D3Q19, and D3Q27, since they offer a sufficient lattice symmetry. The discrete velocity set for the D3Q19 model is shown in Fig. 2.

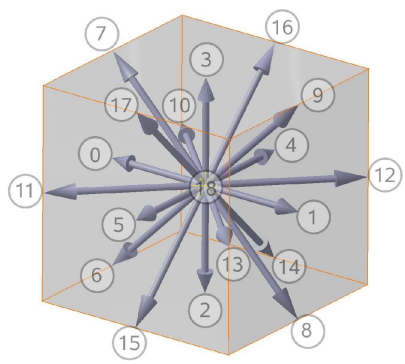

Figure 2: The discrete velocity set of the D3Q19 model.

Since the LBM formulation is based on a uniform Cartesian mesh, it is highly adapted for parallel processing and it offers an efficient boundary treatment for fixed walls. The ability of reproducing variable organic geometries makes this method well suited for biomedical applications.

In this study the flow in the upper human airways was simulated by a D3Q19 LBM-BGK model with a modified equilibrium distribution function for incompressible flows as proposed by Zou et al.[22] Solid wall nonslip boundary conditions were realized by an interpolated bounce-back rule.[23] A Dirichlet boundary condition imposing a fully developed laminar velocity profile was prescribed at the tracheal cross section, whereas a zero gradient condition was employed at the numerous outlets. The computational grid was automatically generated from surface data by an in-house grid generator[15] and consists of 2.5 million cells. It was shown, e. g., in[14] that the numerical method allows a detailed investigation of the three-dimensional flow field in the primary bronchi.

4 RESULTS

The time dependent inhalation and exhalation flow field has been investigated for a peak mass flux of 351 ml/s corresponding to a peak REYNOLDS number of $Re_{max} = 1600$. The value of the REYNOLDS number is based on the hydraulic diameter of the trachea $d_{hyd} = 18.3\,\mathrm{mm}$. To investigate the unsteady behavior of the flow field during respiratory ventilation, simulations and measurements were performed for a normal respiration at rest at frequency f_1 and for a higher respiration frequency $f_2 = 2f_1$. That is, the breathing periods are $T_1 = 4\,\mathrm{s}$ and $T_1 = 2\,\mathrm{s}$ which correspond to WOMERSLEY numbers being defined by $\alpha = 0.5f\sqrt{2\pi f/\nu}$, where the classical notation is used, $\alpha_1 = 3.64$ and $\alpha_2 = 5.15$, respectively.

The temporal variation of the mass flux was prescribed by a sinusoidal curve. The data was recorded after a transient time of one respiration cycle. In the following section numerical and experimental results are compared in a distinct cross section. Subsequently, the numerical data is further analyzed concerning the development of the three-dimensional flow structures.

4.1 Comparison of experimental and numerical data

In this section numerical and experimental data are compared in order to evidence the quality of the LBM solution. A brief comparison is presented for one plane of the first bifurcation which is defined in Fig. 3(a). This region was chosen to globally evidence the mass flux into the lower bifurcations. Moreover, the phase angles at maximum inspiration and expiration can be compared with steady flow cases.

The comparison of the data at α_1 and α_2 shows no significant differences in the flow structures in this plane, which is why in the following only the solutions at $\alpha_1 = 3.64$ are discussed. Fig. 4 contains numerical and experimental results at different phase angels ϕ of a sinusoidal ventilation cycle, where $\phi = 0°$ and $\phi = 180°$ represent maximum inspiration and expiration, respectively. To emphasize the flow direction the vectors possess uniform length. The magnitude of the absolute velocity is normalized on the bulk velocity in cross section I in Fig. 3(b) at maximum inspiration. In the following, the terms *upper* and *lower* denote the upper and lower half of the main bronchi (bronchi principales), respectively. Note that there is a third sub-branch at the end of the posterior right main bronchus. The brief discussion of the numerical and experimental findings for various phase angles $\phi = 0°, 90°, 180°, 270°$ shows the quality of the solutions of the Lattice-Boltzmann method under pulsatile flow conditions.

The numerical and experimental data match satisfactorily. The slight differences of the LBM and PIV data are due to small deviations of the lung model and the original geometry data. Moreover, the discrepancies near the wall appear to be caused by a lack of seeding particles in the flow regimes resulting in a decreased resolution of the velocity distribution. Finally, the boundary conditions of the numerical and the experimental setup

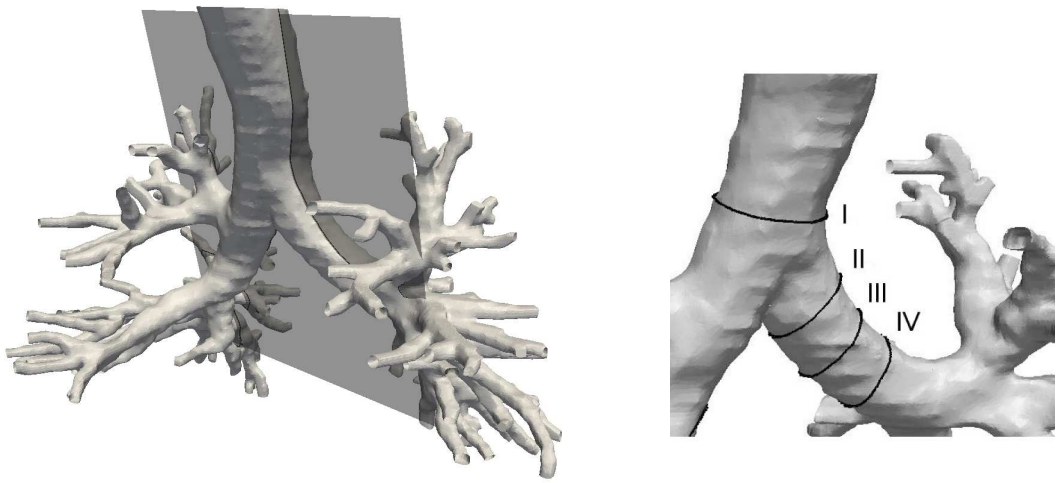

(a) (b)

Figure 3: (a) Reference plane for the comparison of experimental and numerical data; (b) Cross sections for the investigation of secondary flow structures.

do not perfectly coincide, since the pipe extensions downstream of the sixth generation are not taken into account in the simulation and the temporal change of the volume flux is not perfectly sinusoidal in the experiment. Keeping these facts in mind, the numerical-experimental agreement can be considered convincing.

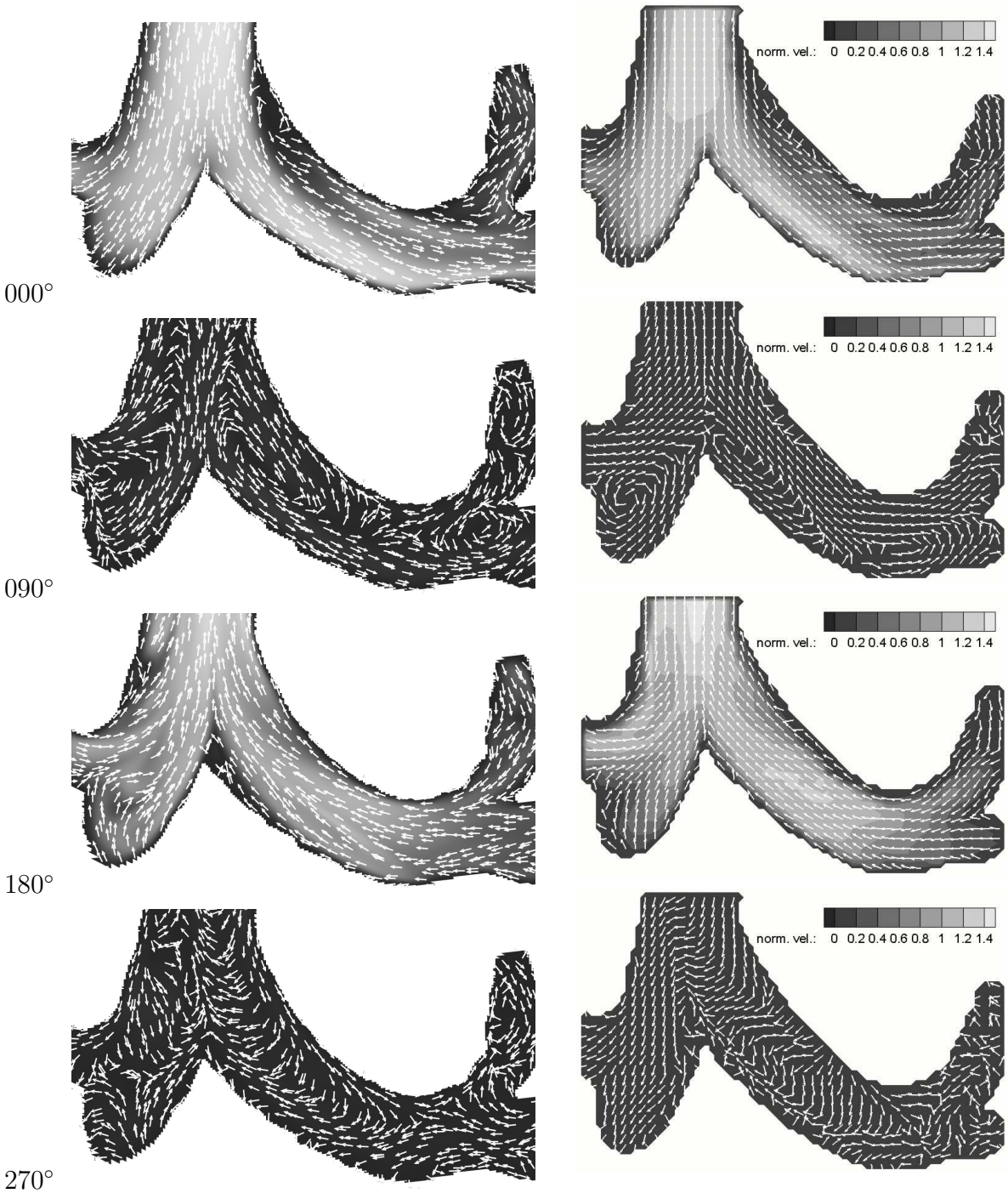

Figure 4: Time resolved data for the second half of a respiration cycle at rest, i. e., $180°, 225°, 270°$ and $315°$; LBM data (left), PIV data (right). The vectors have uniform length and indicate the flow direction. The gray scale values show the magnitude of the absolute velocity that is normalized by the bulk velocity at maximum inspiration for a defined tracheal section.

4.2 Secondary flow structures

In order to obtain a deeper insight into the development of the flow pattern, the secondary flow structures are further analyzed in this section on the basis of the numerical solutions. The locations of the various cross sections denoted by I, II, III, and IV are defined in Fig. 3(b). The flow field in the trachea is depicted for both Womersley numbers in Fig. 5 at maximum inspiration ($\phi = 0°$) and in Fig. 6 at maximum expiration ($\phi = 180°$). The black lines indicate the reference plane of the flow patterns which were discussed in the previous section.

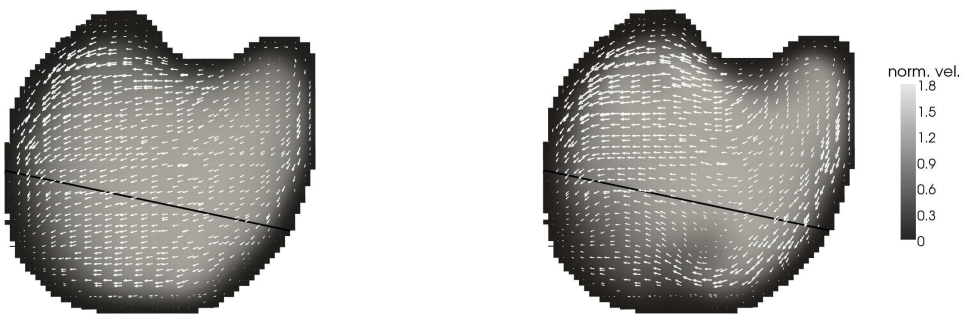

(a) (b)

Figure 5: Flow field in the tracheal cross section I described in Fig. 3(b) at maximum inspiration; (a) $\alpha_1 = 3.64$, (b) $\alpha_2 = 5.15$. The levels of gray indicate the axial velocity magnitude and the arrows represent the in-plane velocity. The black lines indicate the reference plane described in the previous section.

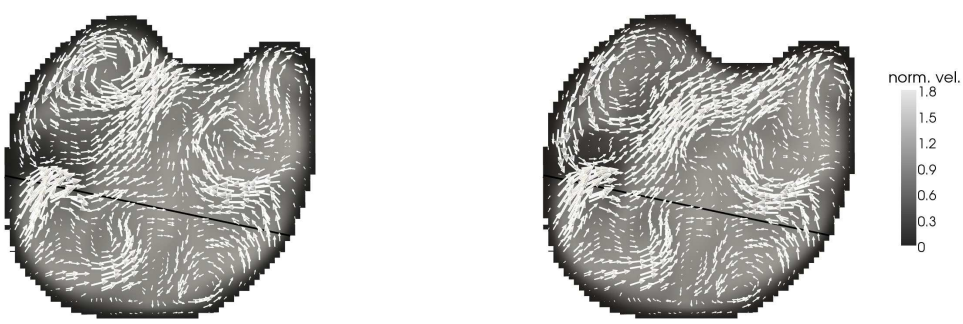

(a) (b)

Figure 6: Flow field in the tracheal cross section I described in Fig. 3(b) at maximum expiration; (a) $\alpha_1 = 3.64$, (b) $\alpha_2 = 5.15$. The levels of gray indicate the axial velocity magnitude and the arrows represent the in-plane velocity. The black lines indicate the reference plane described in the previous section.

At maximum inspiration a well developed velocity profile is observed at α_1 the shape of which is characterized by the geometry of the throat. At α_2 the velocity distribution possesses clear deformations compared to the α_1 profile. At maximum expiration strong vortical structures occur over the whole cross sections which is shown in Fig. 6. These structures are generated by the asymmetric merging of the air streams from the left and right principal bronchus. A stagnation point is observed near the right wall just above the reference plane. Note that unlike the inspiration structures the expiration structures show no significant dependence on the WOMERSLEY number.
In Fig. 7 the flow field at maximum inspiration and expiration at $\alpha_1 = 3.64$ is depicted in the cross sections II, III, and IV.

At inspiration the main mass flux is located near the lower wall. This corresponds to the high velocity region shown in Fig. 4 at $\phi = 0°$. Downstream of the first bifurcation a pair of counter-rotating vortices develops transporting fluid from the high-speed to the low-speed region along the outer walls. The right vortex has a center of rotation near the upper wall and cover most of the upper half of cross section IV. The left vortex is much smaller and it is located very close to the left wall. Such a vortex pair also was observed in the steady state simulations in.[14] The physics of its generation is related to the aforementioned DEAN vortex. Once the next bifurcation is reached, the vortices do separate and each one enters a branch of the next higher bronchial generation.
At expiration the streamwise velocity is more evenly distributed than at inspiration. The mixing of streams coming from the higher generation bronchi generates a shear layer which yields a swirling region. Two stagnation regions are indicated in Fig. 7. One is located at the lower wall and develops in the streamwise direction. The other stagnation region occurs at the left wall and vanishes when the trachea is approached. The in-plane velocity distribution evidences a strong clockwise rotating vortex near to the upper wall and more mass flux is coming from the ventral lung lobe.
In conclusion, the findings confirm pronounced secondary flow structures at inspiration and expiration. The numerical data emphasizes the strong asymmetry of the vortical structures. It is clear that the vortical flow structures are more intricate at expiration ensuring an almost perfect wash-out.

5 SUMMARY AND CONCLUSIONS

The pulsatile flow field in a geometrically realistic model of the human lung was numerically and experimentally investigated for two WOMERSLEY numbers, $\alpha_1 = 3.64$ and $\alpha_2 = 5.15$, and a maximum REYNOLDS number of $Re_{max} = 1600$. The Lattice-Boltzmann method proved to be an accurate tool to simulate flows through highly intricate geometries such as the upper human airways. The numerical findings were validated by particle-image velocimetry measurements. The overall flow structure at inspiration, which is characterized by local recirculation regions, and at expiration, which evidences a more homogeneous velocity distribution, was shown to be in convincing agreement. Secondary flow structures known from steady state simulations were clearly identified. A pair of counter-rotating

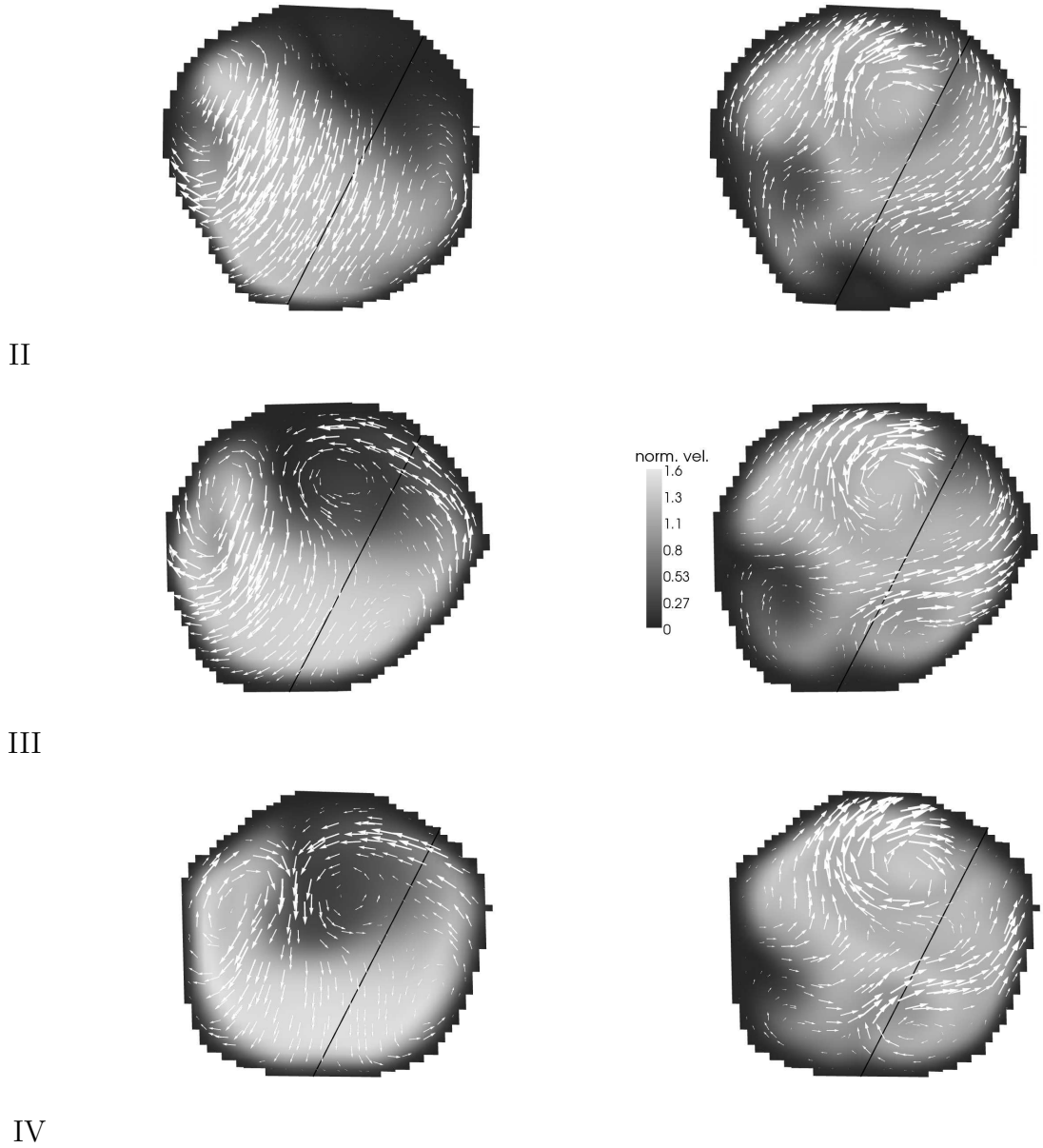

Figure 7: Flow field in the cross sections II-IV; inspiration (left), expiration (right). The axial velocity is shown by gray scale values and the arrows represent the in-plane velocity. The black lines indicate the reference plane described in the previous section.

vortices and a high-speed region were observed downstream of the first bifurcation in the left bronchus.
The results reflect the three-dimensional flow pattern inside the highly complex geometry of a real human lung. This knowledge is essential for the improvement of artificial respiration devices and for the development of aerosol drug delivery systems. In future investigations higher generations of the lung geometry and also the upper airways will be fully modeled including the nasal cavity and the laryngeal region.

6 ACKNOWLEDGMENT

The support of the Deutsche Forschungsgemeinschaft (DFG) is gratefully acknowledged.

REFERENCES

[1] Y. Zhao and Baruch B. Lieber. Steady Expiratory Flow in a Model Symmetric Bifurcation. *Journal of Biomechanical Engineering*, 116(3):318–323, 1994.

[2] J. K. Comer, C. Kleinstreuer, and C. S. Kim. Flow structures and particle desposition patterns in double-bifurcation airway models. Part 1. Air flow fields. *J Fluid Mech*, 435:25 – 54, 2001.

[3] Y. Liu, R. M. C. So, and C. H. Zhang. Modelling the bifurcating flow in a human lung airway. *Journal of Biomechanics*, 35(4):465–473, 2003.

[4] C. van Ertbruggen, C. Hirsch, and M. Paiva. Anatomically based three-dimensional model of airways to simulate flow and particle transport using computational fluid dynamics. *J. Appl. Physiol.*, 98:970–980, 2005.

[5] E.R Weibel. *Morphometry of the Human Lung.* Springer Berlin, 1963.

[6] Z. Zhang, C. Kleinstreuer, and C. S. Kim. Gas-solid two-phase flow in a triple bifurcation lung airway model. *International Journal of Multiphase Flow*, 28(6):1021 – 1046, 2002.

[7] Z. Li, C. Kleinstreuer, and Z. Zhang. Particle deposition in the human tracheobronchial airways due to transient inspiratory flow patterns. *Journal of Aerosol Science*, 38(6):625 – 644, 2007.

[8] N. Nowak, P. P. Kakade, and A. V. Annapragada. Computational Fluid Dynamics Simulation of Airfoil and Aerosol Deposition in Human lungs. *Annals of Biomedical Eng.*, 31:374 – 390, 2003.

[9] Ching-Long Lin, Merryn H. Tawhai, Geoffrey McLennan, and Eric A. Hoffman. Characteristics of the turbulent laryngeal jet and its effect on airflow in the human intrathoracic airways. *Respiratory Physiology & Neurobiology*, 157(2-3):295 – 309, 2007.

[10] S. Große, W. Schröder, M. Klaas, A. Klöckner, and J. Roggenkamp. Time resolved analysis of steady and oscillating flow in the upper human airways. *Experiments in Fluids*, 42:955–970, June 2007.

[11] S. Große, W. Schröder, and M. Klaas. Time-Resolved PIV Measurements of Vortical Structures in the Upper Human Airways. In *Particle Image Velocimetry*, volume 112/2008 of *Topics in Applied Physics*, pages 35–53. Springer Berlin/Heidelberg, 2008.

[12] S. Succi. *The Lattice Boltzmann Equation for fluid dynamics and beyond*. Oxford University Press, Oxford, 2001.

[13] C. G. Ball, M. Uddin, and A. Pollard. Mean flow structures inside the human upper airway. *Flow, Turbulence and Combustion*, 81:155–188, 2008.

[14] Rainhill K Freitas and Wolfgang Schröder. Numerical investigation of the three-dimensional flow in a human lung model. *Journal of Biomechanics*, 2008.

[15] D. Hartmann, M. Meinke, and W. Schröder. An adaptive multilevel multigrid formulation for Cartesian hierarchical grid methods. *Comput. Fluids*, 37:1103–1125, 2008.

[16] U. Frisch, B. Hasslacher, and Y. Pomeau. Lattice-gas automata for the Navier Stokes equation. *Phys. Rev. Lett.*, 56(14):1505–1508, 1986.

[17] R. Benzi, S. Succi, and M. Vergassola. The Lattice Boltzmann Equation: Theory and Applications. *Physics Reports*, 222(No. 3):145–197, 1992.

[18] S. Chen and G D. Doolen. Lattice Boltzmann method for fluid flows. *Annu. Rev. Fluid Mech.*, 30:329 – 364, 1998.

[19] P. L. Bhatnagar, E. P. Gross, and M. Krook. A Model for Collision Processes in Gases. I. Small Amplitude Processes in Charged and Neutral One-Component Systems. *Phys. Rev.*, 94(3):511–525, May 1954.

[20] D. Hänel. *Molekulare Gasdynamik*. Springer, Berlin, 2004.

[21] Y.-H. Qian, D. D'Humieres, and P. Lallemand. Lattice BGK Models for Navier-Stokes Equations. *Europhysics Letters*, 17(6):479 – 484, 1992.

[22] Q. Zou, S. Hou, S. Chen, and G D. Doolen. An improved incompressible lattice Boltzmann model for time-independent flows. *Journal of Statistical Physics*, 81(1–2):35–48, 1995.

[23] M. Bouzidi, M. Firdaouss, and P. Lallemand. Momentum transfer of a Boltzmann-lattice fluid with boundaries. *Physics of Fluids*, 13(11):3452–3459, 2001.